NMR Analysis of Polyester Urethane End Groups and Solid-Phase Hydrolysis Kinetics

David M. LeMaster* and Griselda Hernández

Bioscience Division, Group BS-1, Los Alamos National Laboratory, Los Alamos, New Mexico 87545

Received December 3, 1999; Revised Manuscript Received February 21, 2000

ABSTRACT: Multidimensional heteronuclear solution NMR is used for end group analysis and solid-phase hydrolysis kinetics determination on a 40 kDa commercial linear polyester urethane. Pure autocatalytic acid cleavage of the ester linkages is observed under humid atmosphere. T_1 and T_2 relaxation effects on 2D $^1H-^{13}C$ correlation spectra are analyzed so as to provide quantitative interpretation of cross-peak intensity for relative concentration measurements. A 3D ^{13}C-purged $^1H-^1H-^{13}C$ TOCSY−HSQC experiment serves to establish extensive ^1H and ^{13}C spin coupling connectivities at a level of 1−2 sites per 40 kDa. Spin coupling analysis of (approximately) symmetric monomer units is facilitated by using the natural abundance ^{13}C enrichment to break the local symmetry.

Introduction

Molecular weight determination of linear polymers by NMR requires the quantitation of the end group distribution relative to the internal polymer units. NMR analysis offers the advantage of direct M_N determination in addition to its capability in identification of various end groups structures when competing synthesis and/or cleavage processes are present. Various approaches have been introduced to overcome limitations of sensitivity and resolution in NMR end group analysis. In favorable cases the resolution in 1D ^1H spectra is sufficient to provide quantitation at high sensitivity.[1−5] For situations in which ^{13}C observation is required, isotopic enrichment of the monomers has been used to enhance sensitivity.[6−8] Alternately, radical initiator molecules have been labeled with NMR active nuclei to provide for sensitive end group detection.[9−13] In many cases end groups can be chemically modified to incorporate an NMR-active derivative,[14−17] although concerns regarding the completeness of derivatization need be addressed.[18,19]

Most general are NMR approaches to end group analysis which can exploit the resolution of the ^{13}C spectrum at natural abundance. 1D ^{13}C as well as 2D ^{13}C observe $^{13}C-^1H$ HETCOR[20] and ^1H observe $^1H-^{13}C$ HMQC[21,22] experiments have most commonly been utilized in such studies. COLOC[23] and HMBC[24] experiments have been used to observe long-range $^1H-^{13}C$ spin couplings in polymers as well. In many cases unambiguous end group resonance assignment requires a more extensive set of spin coupling correlations than are provided by these experiments. Herein is demonstrated the utility of ^{13}C-separated $^1H-^1H$ TOCSY experiments for end group identification in natural abundance polymer samples.

Use of cross-peak intensities in multidimensional $^1H-^{13}C$ spectra for estimation of relative concentrations presents several complexities in addition to those faced in using standard 1D ^1H or ^{13}C spectra for quantitative analysis. Compensation for these effects can provide accurate M_N determination as well as more generally serving to facilitate quantitation of covalent structural characteristics. These approaches have been applied to molecular weight estimation and hydrolysis kinetics analysis of polyester urethanes. The increased hydrolytic stability of polyether urethanes has long pointed to the ester linkages as the primary site of hydrolysis in polyester urethanes.[25] Consistent with model ester hydrolysis studies, early pH titration analyses of hydrolysis in polyester urethanes[26] and other polyesters[27] under neutral to slightly acidic conditions have indicated an autocatalytic reaction arising from the generation of a free carboxyl group in each step of hydrolytic cleavage. On the other hand, some more recent studies have argued for noncatalytic or mixed order catalysis for polyester hydrolysis in the solid phase.[28−30] These previous studies generally utilized either pH titration, which is sensitive to the presence of small molecule buffering effects, or gel permeation chromatography, in which corrections for potential changes in polydispersity as a function of degradation need be considered. This question has been reexamined in a polyester urethane system in which the free hydroxyl, carboxyl, and arylamine content of the polymer is directly monitored for cleavage of either ester or urethane linkages.

Experimental Section

Millimeter thick wafers of the polyester urethane Estane 5703 (Goodrich) were incubated at 70 °C in 74% relative humidity for varying periods of time (kindly provided by J. R. Schoonover and E. B. Orler). The wafers were then dried under vacuum for a week against anhydrous $MgSO_4$. Aliquots were dissolved in anhydrous $^2H_6$-dimethyl sulfoxide to a concentration of approximately 5%. NMR measurements were carried out at 55 °C on a Bruker Avance DRX 500 spectrometer equipped with a $\{^1H,^{13}C,^{15}N\}$ triple-resonance, triple-axis gradient probe. Chemical shift referencing was made to the deuterated dimethyl sulfoxide resonances at 2.50 ppm ^1H and 39.5 ppm ^{13}C.

2D $^1H-^{13}C$ correlation spectra were obtained using a refocused INEPT-based sensitivity-enhanced sequence (Figure 3a of ref 31) utilizing a 5 ms ^{13}C T_1 relaxation delay followed by a pulse field gradient which provided enhanced suppression of artifacts relative to a simpler refocused INEPT sequence. Polarization transfer delays of 0.9 ms were used to optimize for the methylene transfer function. The typical collection parameters for the 2D $^1H-^{13}C$ correlation spectra were spectral widths of 15.0 ppm ^1H and 46.0 ppm ^{13}C and digital resolution of 3.66 Hz for ^1H and 2.82 Hz for ^{13}C. For the 2.0 s

* Corresponding author: phone (505)667-6686; FAX (505)667-0110; E-mail lemaster@lanl.gov.

10.1021/ma992030w CCC: $19.00
Published on Web 04/29/2000

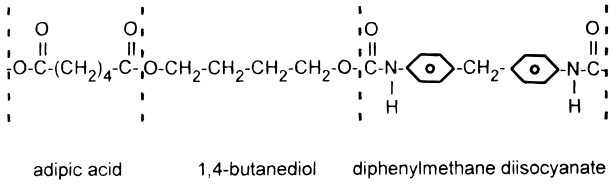

Figure 1. The polyester urethane Estane 5703 is formed by ester linkages between adipic acid and 1,4-butanediol and urethane linkages generated by the reaction between 4,4′-diphenylmethane diisocyanate and 1,4-butanediol.

recycle time used in the unhydrolyzed reference polymer spectra of Figures 2 and 7, 40 scans per t_1 increment yielded a 53 h total acquisition. This refocused INEPT-based sensitivity-enhanced sequence was also used for ^{13}C T_1 measurements, while those same authors' sequence (Figure 3b[31]) was used for the ^{13}C T_2 measurements. $^1H-^{13}C$ dipole cross-correlation effects at these methylene sites[32,33] were not explicitly accounted for in the present relaxation analysis, although only relaxation delay times shorter than the decay constant were used to minimize the influence of the resultant biexponential decay.

The ^{13}C-purged $^1H-^1H-^{13}C$ TOCSY−HSQC experiments used a DIPSI-2rc mix sequence[34] with a 5 kHz ^1H field to suppress ROE contributions during the TOCSY transfer. The 3D experiment utilized spectral widths of 7.0 ppm for both ^1H dimensions and 4.0 ppm for the ^{13}C dimensions. Digital resolution in the indirect dimensions were 7.0 Hz for ^1H and 6.3 Hz for ^{13}C. Using the minimum phase cycle of four scans per increment, a recycle delay of 1.0 s yields a total acquisition time of 73 h.

Results and Discussion

^1H, ^{13}C Spin Coupling Network Assignment in Polyester Urethanes. The linear polyester urethane used in this study is Estane 5703 (Goodrich), which is produced via the reaction of 1,4-butanediol with 4,4′-diphenylmethane diisocyanate and adipic acid as schematized in Figure 1. Each internal butanediol unit forms either an ester or a urethane linkage at each end. Hence, as illustrated in Figure 2A, there are expected to be four distinct $-^{13}CH_2-OR$ butanediol cross-peaks in a $^1H-^{13}C$ 2D correlation spectrum. The pair of upfield resonances arise from proximal ester linkages while the downfield pair arise from nuclei that are adjacent to urethane linkages. Within each of these two pairs of resonances the upfield cross-peak arises from butanediol groups with an ester linkage at the distal end. As compared to the commonly used HMQC experiment, this sensitivity-enhanced refocused INEPT-based HSQC experiment[31] provides superior resolution in the ^{13}C dimension. This improved resolution results from elimination of $^1H-^1H$ spin coupling modulation in the heteronuclear dimension that is present in the HMQC experiment as well as by elimination of scalar relaxation of the second kind arising from ^1H T_1 relaxation.[35]

Terminal butanediol units would be anticipated to give rise to far weaker -$^{13}CH_2-OH$ cross-peaks near the spectral region illustrated in Figure 2B. In analogy to the resonances in panel A, the more intense upfield cross-peak is tentatively assigned to the ester-linked terminal butanediol while the 3.1-fold weaker downfield peak arises from the urethane-linked terminal butanediol units. However, alternate possibilities for the assignment for either of these resonances (e.g., butanediol monomer) cannot be excluded solely on the basis of this 2D correlation spectrum. To directly verify the identification of these cross-peaks, a variant of the standard 3D $^1H-^1H-^{13}C$ TOCSY−HSQC experiment[36] was carried out (Figure 3). In the TOCSY−HSQC experiment the initially excited ^1H resonances are frequency labeled in the evolution period of the first dimension. The ^1H magnetization is then transferred throughout the local $^1H-^1H$ spin coupling network via a TOCSY mixing sequence.[37] An HSQC sequence then transfers magnetization to the directly bonded ^{13}C for frequency labeling of the second dimension and then back to the attached

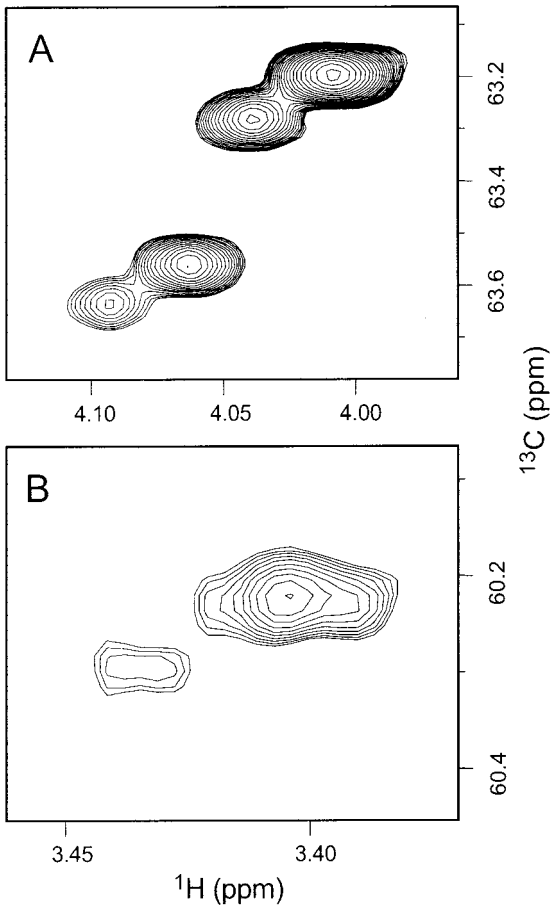

Figure 2. 2D $^1H-^{13}C$ correlation spectra of the $-^{13}CH_2-OR$ methylene resonances of the internal (panel A) and terminal (panel B) butanediol units of the polyester urethane Estane 5703.

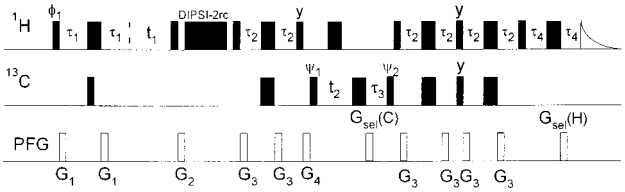

Figure 3. Pulse scheme for a ^{13}C-purged 3D $^1H-^1H-^{13}C$ TOCSY−HSQC experiment. Narrow and wide bars for ^1H and ^{13}C indicate 90° and 180° rf pulses, respectively. The intensity and duration of the pulse field gradients were G_1 (12 G/cm, 1.0 ms), G_2 (14 G/cm, 1.0 ms), G_3 (7 G/cm, 0.5 ms), and G_4 (−15 G/cm, 1.5 ms). The ^{13}C and ^1H coherence selection gradients were applied at magic angle for 1.003 and 0.251 ms with field strengths of 25 and ±25 G/cm, respectively. The rf phases are set to x except where indicated: $\phi_1 = \{x,-x\}$, $\psi_1 = \{x,x,-x,-x\}$, $\psi_2 = \{x\}$, and receiver = $\{x,-x,-x,x\}$. Quadrature detection in t_1 is obtained with the States-TPPI technique[48] by incrementation of ϕ_1. Sensitivity-enhanced quadrature discrimination in t_2 is obtained utilizing the echo−antiecho technique.[49,50] For each t_2 value the two quadrature components were obtained by 180° shifts on ψ_2 while ψ_1 is shifted 180° for each t_2 increment. Delay times $\tau_1 = 3.5$ ms, $\tau_2 = 1.75$ ms, $\tau_3 = 1.5$ ms, and $\tau_4 = 500$ μs were used.

^{1}H for observation. In the experiment described in Figure 3, the first ^{1}H 90° pulse is followed by a ^{13}C purge sequence.[38,39] This ^{13}C purge component serves to eliminate initial ^{1}H signal which is bound to ^{13}C. In contrast, the HSQC component at the end of the sequence selects for only ^{1}H signals attached to ^{13}C. As a result, ^{1}H magnetization which remains on the same nucleus during the TOCSY mixing time (i.e., the intense diagonal peaks) is strongly suppressed.

In the left-hand panel of Figure 4 is illustrated a portion of the 2D ^{1}H−^{1}H plane from the 3D ^{13}C-purged ^{1}H−^{1}H−^{13}C TOCSY−HSQC data set sliced at a ^{13}C chemical shift of 63.20 ppm which corresponds to the $-^{13}\mathbf{C}H_2-$OR resonance for the symmetric diadipate-linked internal butanediol units. At (4.0, 1.6) ppm is the resonance which arises from ^{1}H magnetization initially residing on the two equivalent central methylenes of the internal butanediol and subsequently transferred during the 80 ms TOCSY mixing period to the $-^{13}C\mathbf{H}_2-$OR resonance. The large diagonal peak at (4.0, 4.0) ppm arises exclusively from ^{1}H magnetization which has been relayed from one end of the butanediol unit to the other during the TOCSY mixing period. Since there was no ^{13}C decoupling applied during the first ^{1}H evolution period, any $-^{13}C\mathbf{H}_2-$OR magnetization which did not transfer during the TOCSY mixing period will be split by the 140 Hz ^{1}H−^{13}C coupling constant in the indirect (vertical) ^{1}H dimension. The weak satellite peaks on either side of the (4.0, 4.0) ppm peak arise from the nonrelayed ^{13}C bound ^{1}H magnetization which is not completely suppressed by the ^{13}C purge component.

In the right-hand panel of Figure 4 at a much lower contour are illustrated the weaker ^{1}H−^{1}H TOCSY cross-peaks in the ^{13}C slice at 60.2 ppm which corresponds to the $-^{13}\mathbf{C}H_2-$OH resonance for the adipate-linked terminal butanediol units. For the sensitivity level of this experiment, no ^{13}C satellites of the diagonal peak are apparent near (3.4, 3.4) ppm reflecting the relatively efficient ^{13}C purge component. On the other hand, cross-peaks are apparent at (3.4, 4.0) and (3.4, 1.6) ppm consistent with ^{1}H magnetization relayed across three and two vicinal ^{1}H−^{1}H couplings, respectively, for an adipate-linked butanediol terminus. The cross-peak at (3.4, 1.45) ppm corresponds to the chemical shift expected for initial excitation of the $-C\mathbf{H}_2-^{13}CH_2-$OH resonance followed by TOCSY relay to the terminal butanediol methylene.

Hence, direct covalent connectivity can be demonstrated across the entire terminal butanediol unit at a sensitivity of 1−2 sites per 40 kDa (see below) in a natural abundance commercial polymer sample. This experiment can be anticipated to provide comparable covalent connectivity information in polymer synthesis and degradation applications in which the chemical identity of individual 2D cross-peaks is less readily apparent.

The practical benefits of suppression of the diagonal peaks in the ^{13}C-purged ^{1}H−^{1}H−^{13}C TOCSY−HSQC experiment are more clearly illustrated in Figure 5. In this figure the 3D data set has been sliced at the ^{13}C frequencies of 63.61 (blue) and 63.24 ppm (green), showing the expanded 2D ^{1}H−^{1}H diagonal region containing the internal butanediol $-C\mathbf{H}_2-$OR resonances. These two ^{13}C slices have been overlaid to more easily compare the relative ^{1}H chemical shifts. The 63.61 ppm ^{13}C slice lies between the downfield resonances of Figure 2A which arise from the urethane-linked

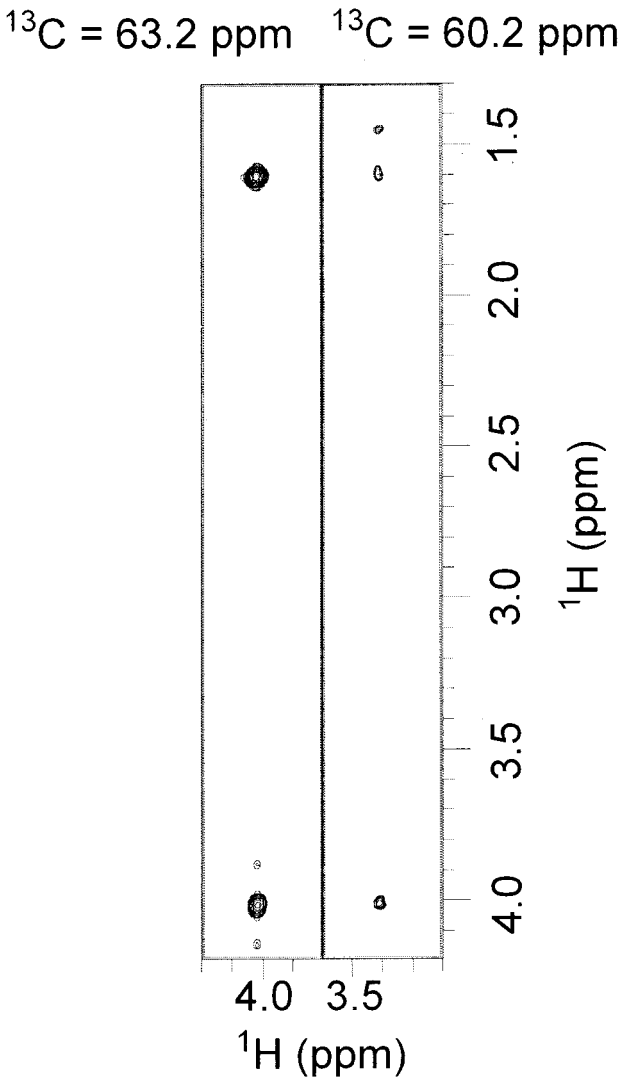

Figure 4. Butanediol cross-peak region of 2D ^{1}H−^{1}H planes taken from a 3D ^{13}C purged ^{1}H−^{1}H−^{13}C TOCSY−HSQC experiment using an 80 ms mix time. The left-hand panel is a ^{13}C slice at 63.2 ppm which corresponds to the $-^{13}\mathbf{C}H_2-$OR resonance for the diadipate-linked internal butanediol units. The (4.0, 4.0) ppm diagonal peak arises from magnetization transferred from one end to the other of the internal butanediol unit. As no ^{13}C decoupling is applied during the evolution of the indirect ^{1}H dimension, the weak satellite peaks around the diagonal arise from incomplete ^{13}C purging of the initial ^{1}H magnetization. The peak at (4.0, 1.6) ppm arises from initial ^{1}H magnetization on the central two methylene positions which is subsequently relayed to the $-^{13}C\mathbf{H}_2-$OR resonance. The right-hand panel is a ^{13}C slice at 60.2 ppm which corresponds to the $-^{13}\mathbf{C}H_2-$OH resonance for the adipate-linked terminal butanediol units. Because of the ^{13}C purge component, the ^{13}C coupled doublet anticipated around the diagonal at (3.4, 3.4) ppm is not observed at this sensitivity. The resonances at 1.45, 1.6, and 4.0 ppm correspond to the ^{1}H chemical shifts expected for the three other butanediol methylene positions extending in order away from the terminal methylene.

butanediol ends, while the 63.24 ppm ^{13}C slice lies between the resonances for the adipate-linked butanediol ends. For each ^{1}H chemical shift of the four different internal butanediol $-C\mathbf{H}_2-$OR resonances seen in Figure 2A, there are weak satellite peaks in Figure 5 that lie on either side of the diagonal separated by the 140 Hz ^{1}H−^{13}C coupling. These arise from the incompletely purged ^{13}C bound ^{1}H magnetization which was not transferred during the TOCSY mixing period.

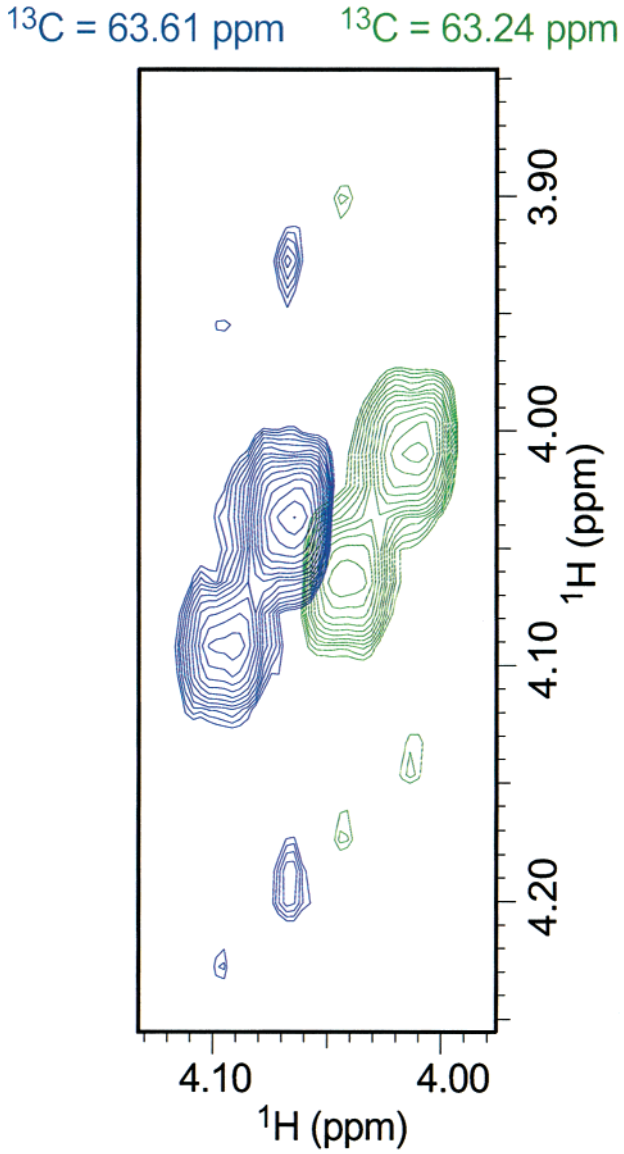

Figure 5. An expansion of the 3D ^{13}C-purged ^{1}H−^{1}H−^{13}C TOCSY−HSQC spectrum in Figure 4 which contains the diagonal region of the internal butanediol −C**H**$_2$−OR resonances. Two different ^{13}C slices at 63.61 (blue) and 63.24 ppm (green) are overlaid for comparison. The more intense peaks near the diagonal arise exclusively from magnetization relayed between the ends of the butanediol units. The two diagonal peaks at (4.01, 4.01) and (4.09, 4.09) ppm arise from the symmetric diester- and diurethane-linked butanediol units, respectively. The central two resonances at (4.04, 4.07) and (4.07, 4.04) ppm are off-diagonal, thus demonstrating that they arise from magnetization relayed across the asymmetric urethane−butanediol−adipate linked units. Note that the positioning of the ^{13}C slices and relative intensity scaling of the two spectra have been selected to yield similar intensities for the four relayed peaks as well as for the weak ^{13}C satellite peaks arising from incomplete ^{13}C purging.

The four intense peaks near the diagonal all arise exclusively from magnetization which has been transferred between the methylenes at either end of the internal butanediol unit. The diagonal peaks at (4.01, 4.01) and (4.09, 4.09) ppm arise from the symmetric diester- and diurethane-linked butanediol units, respectively. The off-diagonal cross-peaks at (4.04, 4.07) and (4.07, 4.04) ppm can only arise from magnetization which has been transferred between the nonequivalent ends of the asymmetric adipate−butanediol−urethane-linked units. As expected, the intensities of the (near) diagonal vs satellite peaks are strongly dependent on the TOCSY mix time. The central resonances arising from the magnetization which has been transferred across the butanediol unit are far weaker when a short (8 ms) mix time is used, reflecting the inadequate time for efficient multistep scalar coupling transfer.

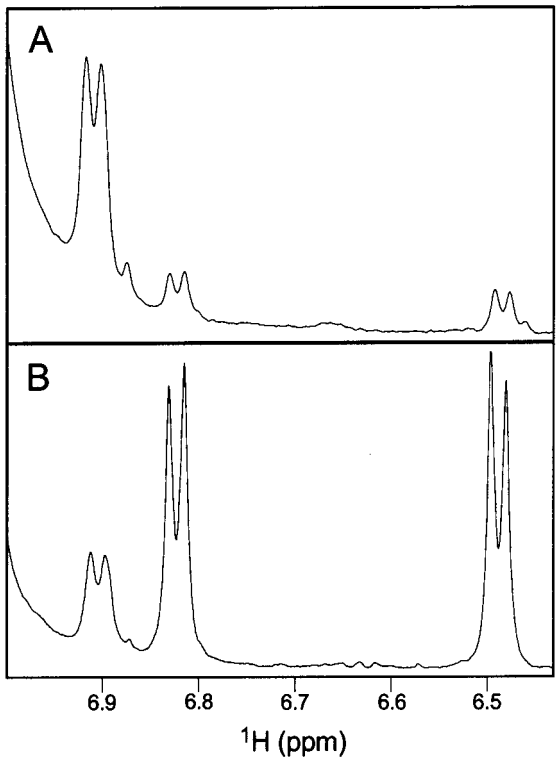

Figure 6. 1D ^{1}H NMR spectrum of a portion of the aromatic region containing the ortho (6.48 ppm) and meta (6.83 ppm) resonances of the arylamine end groups of Estane 5703. Also evident is the ^{13}C satellite of the ortho resonance of the internal diphenylmethane units at 6.91 ppm. In panel A is the spectrum obtained from the reference polyester urethane sample, while in panel B is given the spectrum from this sample hydrolyzed at 70 °C for 2 weeks in 95% ^{2}H$_6$-dimethyl sulfoxide/5% ^{2}H$_2$O.

Approximate local symmetries are common features in many commercial polymers. The present results demonstrate the practicality of using the natural abundance distribution of ^{13}C to break these local symmetries and thus establish covalent connectivities between the (near) equivalent ^{1}H resonances. In the absence of such a ^{13}C purge−^{13}C selection technique the intense diagonal ^{1}H−^{1}H peaks will generally overwhelm the smaller relayed peaks of similar ^{1}H chemical shift.

Quantitation of Polymer End Group Distribution. Quantitation of the arylamine end groups is most straightforward, as these give rise to well-resolved 1D ^{1}H resonances which can be reliably integrated using long recycle delays to eliminate resonance saturation effects. Arylamine end groups arise from either hydrolysis of the isocyanate groups during polymerization or from subsequent hydrolysis of the urethane linkages. As illustrated in the unhydrolyzed reference polyester urethane spectrum (Figure 6A), the upfield shifted arylamine ^{1}H resonances (6.48 and 6.83 ppm, ortho and meta, respectively) are readily resolved from the aromatic ^{1}H envelope. Using the urethane linkage hydrolyzed sample discussed below, 2D ^{1}H−^{13}C correlation spectra yielded 114.1 and 128.9 ppm for the corresponding ortho and meta arylamine ^{13}C resonances, which agree closely with the ^{1}H and ^{13}C shifts of the model

Table 1. Estimation of Butanediol-$^{13}CH_2OR$ Intensities

	2.0 s recycle	3.6 s recycle	∞ recycle[a]	T_2 corrected[b]
internal/terminal	239	204	195	203

[a] The 2.0 and 3.6 s recycle delay values indicate an apparent 1.2 s differential decay time. This value was used to estimate the intensity ratio for a fully relaxed spectrum. [b] The ~100 and 200 ms ^{13}C T_2 relaxation times for the internal and terminal resonances, respectively, were used to estimate 8% (internal) and 4% (terminal) relaxation effects during the polarization transfer delays.

compound *p*-aminotoluene. The ^1H resonance at 6.91 ppm in Figure 6 is the ^{13}C satellite of the ortho ^1H aryl signal of the internal diphenylmethane units. As the satellite peak (0.55% of parent ^{12}C peak) is 5 ±1 times larger than the arylamine peaks, the ratio of internal to terminal diphenylmethane peak intensities is 1000/1. There are four ortho protons per symmetric diphenylmethane internal monomer unit while there are only two ortho (or meta) protons in each terminal arylamine unit. However, since there are two ends to the linear polymer, the ratio of internal to terminal diphenylmethane units is also 1000/1.

Four potentially significant sources of error must be considered in quantitating heteronuclear correlation spectra: the coupling constant dependence of $^1H-^{13}C$ polarization transfer, resonance offset effects, ^1H T_1 relaxation during recycle delays, and T_2 relaxation during polarization transfer delays. In the present study the primary focus is on the normalization of the terminal butanediol $-\mathbf{CH}_2-OH$ resonances against the internal butanediol $-\mathbf{CH}_2-OR$ resonance intensities. The one bond $^1H-^{13}C$ coupling constants are similar for both, while the 3 ppm difference between these ^{13}C resonances is small compared to the 18.5 kHz ^{13}C rf field used. Hence, neither the coupling constant dependence of $^1H-^{13}C$ polarization transfer nor resonance offset effects are anticipated to significantly affect determination of this intensity ratio. However, it should be noted that the presence of multiple 180° ^{13}C pulses in these 2D correlation experiments increases the resonance offset effects relative to the small-angle excitations commonly used in 1D experiments. In general, duplicate experiments using different excitation frequencies can be used to quantitate variation in peak intensities as a function of offset.

To correct for incomplete ^1H T_1 relaxation between scans, 2D $^1H-^{13}C$ correlation spectra were collected using recycle delay times of 2.0 and 3.6 s. As summarized in Table 1, the ratio of the $-\mathbf{CH}_2-OR/-\mathbf{CH}_2-OH$ peak volumes were 239 and 204, respectively, consistent with the expected longer ^1H T_1 times for the more mobile terminal butanediol. These values yield an apparent 1.2 s differential decay time with a resultant estimate of 195 for the ^1H T_1 relaxation corrected $-\mathbf{CH}_2-OR/-\mathbf{CH}_2-OH$ peak volume ratio.

Correction for T_2 relaxation effects during the refocused INEPT polarization transfer steps is more problematic. Analogous to the ^1H T_1 relaxation correction, the $-\mathbf{CH}_2-OR/-\mathbf{CH}_2-OH$ peak volume ratio can be determined as a function of decreasing polarization transfer delays followed by extrapolation to a zero delay. Unfortunately, the peak intensities decrease rapidly for transfer delays much shorter than optimal. In the present application variation of the transfer delay period yielded results consistent with the T_2 correction being less than 10%; however, as discussed below, the S/N of the end group peak is not sufficient for a more robust estimate.

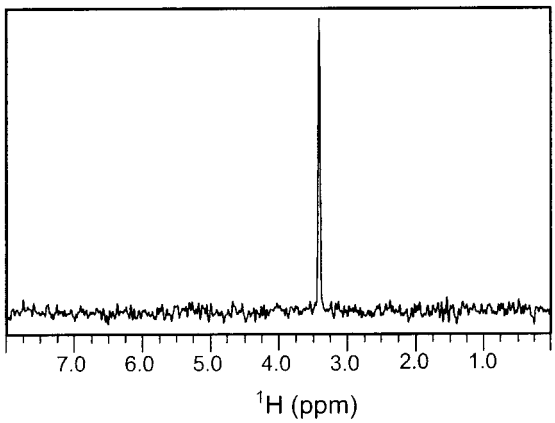

Figure 7. 1D ^1H slice from the 2D $^1H-^{13}C$ correlation spectrum of Estane 5703 selected at the ^{13}C frequency of the cross-peak from the adipate-linked terminal butanediol $-\mathbf{^{13}C}H_2-OH$ at 60.2 ppm.

An alternate approach involves direct estimation of the relaxation effects for the more intense internal butanediol resonance. During the first two polarization transfer delays of the refocused INEPT sequence, a combination of in-phase and antiphase ^1H T_2 relaxation occurs. Similarly, in the latter two refocusing delay intervals, relaxation effects arise from decay of the in-phase and antiphase ^{13}C T_2 coherences. Although in principle each of these individual contributions can be measured, for dipole vectors undergoing motion in the range of the Larmor frequency (i.e., ~1 ns^{-1} for ^{13}C) as in the present case, the antiphase relaxation is only modestly faster than the in-phase relaxation.[40,41] For the methylene positions the ^{13}C T_2 relaxation is dominated by the two directly attached ^1H dipoles. Correspondingly, the ^1H T_2 relaxation is primarily determined by the directly attached ^{13}C dipole and the geminal $^1H-^1H$ dipole which are of similar magnitude. Hence, the methylene ^1H and ^{13}C T_2 values will generally be roughly equal. To the level of accuracy justified by the rest of the present analysis, the relaxation loss in the refocused INEPT polarization transfer steps can be approximated by the in phase ^{13}C T_2 relaxation rate.

The ^{13}C T_2 relaxation rate for the internal diadipate-linked butanediol $-\mathbf{CH}_2-OR$ resonance was determined to be approximately 100 ms. An independent estimate can be derived from the ^{13}C line width in the 2D correlation spectra for this resonance which indicates a lower limit of 85 ms for the T_2 relaxation time. The eight 0.90 ms polarization transfer delay periods lead to an estimated 8% relaxation loss. An approximately 2-fold longer ^{13}C T_2 relaxation time for the terminal butanediol $-\mathbf{CH}_2-OH$ resonance yields an estimated net differential relaxation effect of 4% during the polarization transfer delays. This results in a final estimate for the $-\mathbf{CH}_2-OR/-\mathbf{CH}_2-OH$ peak volume ratio of 203. As noted below, a substantial uncertainty (~±4%) is ascribed to this estimate.

Regarding the sensitivity of these butanediol end group quantitation experiments, in Figure 7 is given the ^1H 1D slice through the 2D $^1H-^{13}C$ correlation cross-peak for the adipate-linked terminal butanediol $-\mathbf{CH}_2-OH$ resonance. The S/N value of 35 indicates a precision of approximately 3% for the $-\mathbf{CH}_2-OR/-\mathbf{CH}_2-OH$ peak volume determinations. In this natural abundance sample the full intensities of the correspond-

ing parent ^{1}H peaks are 91 (^{13}C enrichment) × 239 (internal vs terminal butanediol ratio) × 35 (S/N of $-\mathbf{CH}_2-$OH peak) = 0.8 × 10^6 times greater than the noise level in Figure 7, thus indicating nearly a millionfold suppression of these signals due primarily to the pulse field gradient selection used in this 2D ^{1}H−^{13}C correlation experiment. The sensitivity observed herein suggests that M_N determinations should be feasible for molecular weights in excess of 100−200 kDa for polymer samples with comparable line widths and relaxation times.

The adipate free acid $-\mathbf{CH}_2-$COOH end group cross-peak overlaps with the tail of the much larger corresponding internal ester cross-peak. In the unhydrolyzed reference polyester urethane sample this free acid ^{1}H−^{13}C cross-peak was not reliably distinguishable. An estimate of approximately 10% initial free acid ends was obtained by analysis of the hydrolysis data as discussed below.

Having determined the relative concentrations for each of the three end group types, the ratios of the internal monomer unit types then yields a M_N value. As there is baseline resolution for their characteristic resonances at 500 MHz, ^{1}H NMR directly indicates monomer distributions of 4.76/3.76/1.00 for butanediol:adipate:diphenylmethane. Integration of the ^{1}H−^{13}C cross-peaks in Figure 2A yields similar results within 2%. The ratio of terminal butanediol groups/arylamines is then 4.76 × (1000 = ratio of internal to terminal aryl groups)/(203 = ratio of internal to terminal butanediol groups) = 23.4. Given a value of 10% free acid end groups, these data yield an end group distribution of 86.3/10/3.7 for the hydroxyl:acid:arylamine end groups. In turn this implies an average of 175 internal butanediol, 138 internal adipate, and 37 internal diphenylmethane units. Ignoring the end group corrections, a M_N value of 40.2 kDa is obtained. Experimental contributions to the uncertainty in the M_N value are estimated to be 2% for the ratio of internal monomer types, 3% for the T_1 corrected internal to terminal butanediol ratio, 4% for the T_2 correction to the internal to terminal butanediol ratio, and 3% for the free acid group concentration. Assuming uncorrelated errors, an aggregate uncertainty of 6−7% in the M_N value is obtained.

Solid-Phase Hydrolysis Kinetics of a Polyester Urethane. In principle, hydrolysis of this polymer can occur at either the ester or urethane linkages. The solution-phase kinetics of esters and urethanes derived from model hydrolysis studies are markedly different. Base-catalyzed hydrolysis of esters and mono-N-substituted urethanes occurs with similar rate constants.[42,43] Acid-catalyzed hydrolysis of esters is also comparatively efficient. Furthermore, under weakly acidic conditions ester hydrolysis is autocatalytic due to the free carboxyl groups generated in the reaction. In contrast, acid hydrolysis of urethanes is far less efficient, becoming significant only below pH 1−2.[44] Neutral solvent-catalyzed urethane hydrolysis is dominant from pH 1−2 up to near neutrality.[45,46]

As a preliminary test of hydrolysis kinetics, ^2H_2O was added to a $^2H_6$-dimethyl sulfoxide solution of Estane 5703 to a final concentration of 5% and incubated at 70 °C for varying time periods. After 2 weeks the spectrum illustrated in Figure 6B was obtained indicating a 15-fold increase in the arylamine resonances. An approximately equal increase in the amount of terminal butanediol end groups was verified from both 1D ^{13}C spectra and the corresponding 2D ^{1}H−^{13}C cross-peaks. Hence, the large majority of hydroxyl end groups generated from hydrolysis arose from urethane cleavage. A tentative rationalization for the limited ester hydrolysis under these conditions may stem from the release of weakly basic arylamine groups which could serve to inhibit the onset of autocatalytic ester hydrolysis. Although these solution-phase hydrolysis results were not pursued in detail, they provide a caution to the common assumption of hydrolysis at the ester linkages.

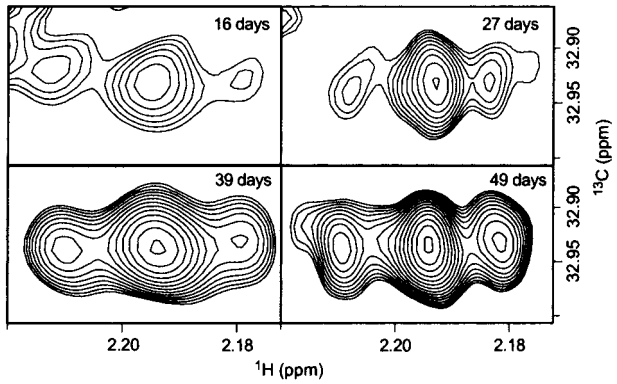

Figure 8. Section of the 2D ^{1}H−^{13}C correlation spectrum containing the free adipate end groups for polyester urethane samples aged 16, 27, 39, and 49 days at 70 °C in 74% relative humidity. Peak distortions in the upper left-hand corner of each spectrum arise from the nearby much more intense internal ester resonance.

To assess both the kinetics and specificity of hydrolysis in the solid phase, NMR analysis was carried out on a series of polyester urethane samples which had been aged at 70 °C in 74% relative humidity for 16, 27, 39, and 49 days. 1D ^{1}H NMR analysis of the arylamine resonances yielded variations of ∼20% in the arylamine end group fraction relative to that of the unhydrolyzed reference sample (i.e., 0.7% of the total end group distribution). However, no systematic increase was observed. Thus, under these conditions of hydrolysis in the solid phase, cleavage of urethane to arylamine end groups is comparatively negligible.

As illustrated in Figure 8, a triplet resonance near the large $-\mathbf{CH}_2-$COOR ester resonance was found to increase as a function of the aging time. The chemical shift agrees with that expected of a methylene adjacent to a terminal free carboxyl. The corresponding cross-peak was not clearly distinguishable in the reference sample. Because of the overlap with the tail of the large $-\mathbf{CH}_2-$COOR resonance, quantitation of the $-\mathbf{CH}_2-$COOH resonance was deemed less reliable than that of the butanediol $-\mathbf{CH}_2-$OH resonance so that the latter was primarily used for the analysis of hydrolysis kinetics.

In Figure 9A is illustrated the increase in the intensity of the butanediol $-\mathbf{CH}_2-$OH resonances as a function of aging time relative to the unhydrolyzed reference sample. An approximate exponential rise in free butanediol ends is apparent as would be expected from an autocatalytic reaction. Given that only a small fraction of the ester groups are being hydrolyzed in this time frame, a pure autocatalytic reaction will follow a simple exponential time course.

Since initial free carboxyl concentration in the unhydrolyzed reference sample could not be determined independently from the NMR data, it was treated as a

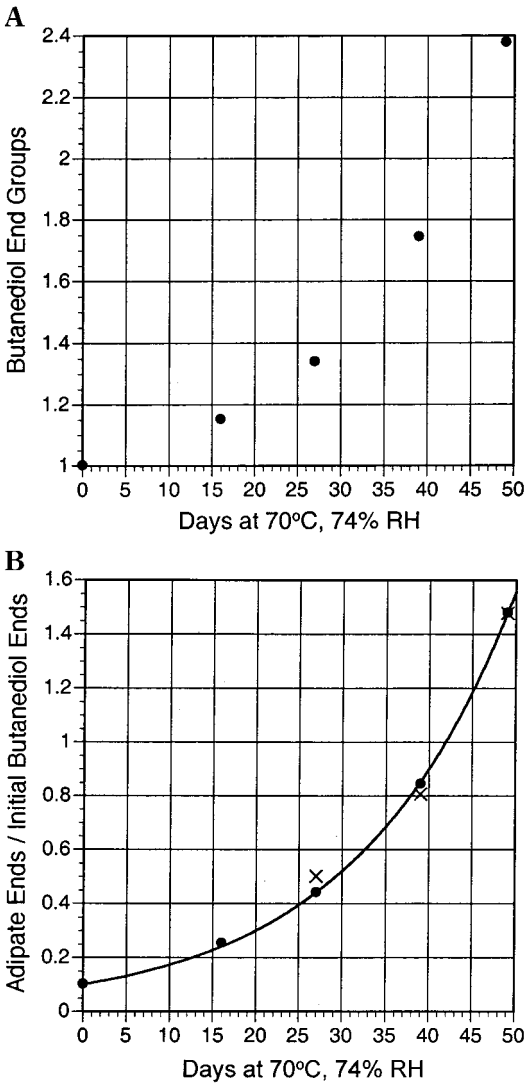

Figure 9. Panel A illustrates the relative increase in butanediol end groups as a function of aging at 70 °C in 74% relative humidity. These estimates are based on the integration of the 2D $^{1}H-^{13}C$ correlation cross-peaks for the terminal butanediol $-^{13}\mathbf{CH_2}-OH$ resonances vs internal butanediol $-^{13}\mathbf{CH_2}-OR$ resonances. In panel B is illustrated the corresponding estimate of the rise in free acid end groups as a function of aging. Given the observed near constancy in the free arylamine group concentration, only ester hydrolysis is assumed to occur, and the initial free acid concentration is estimated by optimizing the fit of the data to the exponential dependence of autocatalysis kinetics. The crosses indicate an independent estimate of the free acid group concentrations based on the intensity of the $-\mathbf{CH_2}-COOH$ cross-peak. Assuming the equality of the butanediol and adipate derived values for the 49 day hydrolysis sample, the free acid end concentrations at 27 and 39 days were determined from the difference in intensity of the corresponding $-\mathbf{CH_2}-COOH$ cross-peaks.

variable in the fit to the data. The optimal fit of the terminal butanediol intensities to an exponential time dependence was obtained when the initial free acid is set to a value of 10%. Using the terminal butanediol intensity data of panel A, in panel B is given the concentration of free acid end groups as a function of aging assuming only ester hydrolysis is occurring. Given the M_N value of 40 kDa, the initial free acid end group value of 10% corresponds to an initial free acid content of 5 μequiv/g, which is similar to estimates derived from pH titration studies of closely related commercial polyester urethane samples.[26]

An independent check of this analysis can be obtained from integration of the free adipate $-\mathbf{CH_2}-COOH$ resonance. Although the lack of a flat base plane due to the partial overlap with the intense internal ester resonance precludes reliable absolute intensities, ideally the intensity increase between time points in the hydrolysis series should be identical for both the butanediol $-\mathbf{CH_2}-OH$ and the adipate $-\mathbf{CH_2}-COOH$ resonances. The free acid end concentration of the 49 day hydrolysis sample for the $-\mathbf{CH_2}-COOH$ resonance was set equal to the free acid end concentration estimated from analysis of the $-\mathbf{CH_2}-OH$ resonance. The crosses in Figure 9B mark the free acid end concentrations which were then deduced from the intensities of the $-\mathbf{CH_2}-COOH$ resonance in the 27 and 39 day hydrolysis samples. Although surely less precise than the butanediol $-\mathbf{CH_2}-OH$ intensity data, the adipate $-\mathbf{CH_2}-COOH$ data clearly support the exponential dependence indicative of autocatalysis as well as supporting the conclusion of effectively exclusive ester hydrolysis.

The indirect prediction of an initial free acid content of 10% cannot be considered to be nearly as reliable as the estimates for the initial hydroxyl and arylamine end groups. However as noted above, under the assumption of an initial free acid content of 10%, an M_N estimate of 40.2 kDa is obtained. A 3% variation in the initial free acid estimate alters this M_N prediction by 3%. Given that 86% of the initial end groups are hydroxyls and 10% are carboxyls, a 2-fold increase in end groups (50% hydroxyl and 50% carboxyl) occurs at 0.68 in Figure 9B. Hence, M_N is reduced by half after 35 days of hydrolysis under these conditions. It should be noted that this half-time estimate is quite insensitive to the initial fraction of carboxyl ends assumed. Values of either 7% or 13% for the initial free acid end group content yield predictions of cleavage half-times within 1 day of that obtained assuming 10%. This 35 day hydrolysis half-time at 70 °C in 74% relative humidity compares favorably with the 25−30 day hydrolysis half-time at 70 °C for wafer samples of closely related Estane polyester urethanes incubated in water.[47]

Conclusions

2D $^{1}H-^{13}C$ correlation spectra has been used to reliably estimate polymer end group concentrations at high sensitivity. This approach is particularly robust for differential measurement of the same cross-peaks as a function of synthesis or aging conditions when variations in relaxation behavior can potentially be minimized. In the more general case of comparing intensities of groups with significantly differing relaxation behavior, correction for the differential relaxation effects can be determined. The ability to establish extensive ^{1}H, ^{13}C spin coupling correlations at natural abundance to the level of 1−2 sites per 40 kDa should markedly facilitate characterization of minor structural variations in polymers arising via either synthesis or degradation. The practical use of natural abundance ^{13}C enrichment to break local symmetries can provide an effective means of overcoming resonance assignment problems arising from spectral degeneracy.

References and Notes

(1) Bevington, J. C. *Fortschr. Hochpolym. Forsch.* **1960**, *2*, 1.
(2) Hatada, K.; Kitayama, T.; Masuda, E. *Polym. J.* **1986**, *18*, 395.

(3) Bignotti, F.; Sozzani, P.; Ranucci, E.; Ferruti, P. *Macromolecules* **1994**, *27*, 7171.
(4) Pasch, H.; Hiller, W. *Macromolecules* **1996**, *29*, 6556.
(5) Hatada, K.; Kitayama, T.; Ute, K.; Terawaki, Y.; Yanagida, T. *Macromolecules* **1997**, *30*, 6754.
(6) Hensley, D. R.; Goodrich, S. D.; Huckstep, A. Y.; Harwood, H. J.; Rinaldi, P. L. *Macromolecules* **1995**, *28*, 1586.
(7) Saito, T.; Rinaldi, P. L. *J. Magn. Reson.* **1998**, *130*, 135.
(8) Becker, H.; Spreitzer, H.; Ibrom, K.; Kreuder, W. *Macromolecules* **1999**, *32*, 4925.
(9) Bevington, J. C.; Ebdon, J. R.; Huckerby, T. N.; Hutton, N. W. E. *Polymer* **1982**, *23*, 163.
(10) Moad, G.; Solomon, D. H.; Johns, S. R.; Willing, R. I. *Macromolecules* **1982**, *15*, 1188.
(11) Bevington, J. C.; Breuer, S. W.; Huckerby, T. N. *Polym. Commun.* **1984**, *25*, 260.
(12) Zambelli, A.; Longo, P.; Pellecchia, C.; Grassi, A. *Macromolecules* **1987**, *20*, 2035.
(13) Saito, T.; Rinaldi, P. L. *J. Magn. Reson.* **1998**, *132*, 41.
(14) Manatt, S. L.; Lawson, D. D.; Ingham, J. D.; Rapp, N. S.; Hardy, J. P. *Anal. Chem.* **1966**, *38*, 1063.
(15) Ho, F. F. L. *Anal. Chem.* **1973**, *45*, 603.
(16) Chan, K. P.; Argyropoulos, D. S.; White, D. M.; Yeager, G. W.; Hay, A. S. *Macromolecules* **1994**, *27*, 6371.
(17) Ronda, J. C.; Serra, A.; Mantecon, A.; Cadiz, V. *Macromol. Chem. Phys.* **1994**, *195*, 3459.
(18) Jankova, K.; Kops, J. *J. Appl. Polym. Sci.* **1994**, *54*, 1027.
(19) Mizawa, T.; Takenaka, K.; Shiomi, T. *J. Polym. Sci., Part A* **1999**, *37*, 3464.
(20) Bax, A.; Morris, G. A. *J. Magn. Reson.* **1981**, *42*, 501.
(21) Mueller, L. *J. Am. Chem. Soc.* **1979**, *101*, 4481.
(22) Bax, A.; Griffey, R. H.; Hawkins, B. L. *J. Magn. Reson.* **1983**, *55*, 301.
(23) Kessler, H.; Griesinger, C.; Zarbock, J.; Loosli, H. R. *J. Magn. Reson.* **1984**, *57*, 331.
(24) Bax, A.; Summers, M. F. *J. Am. Chem. Soc.* **1986**, *108*, 2093.
(25) Schollenberger, C. S.; Stewart, F. D. *J. Elastoplast.* **1971**, *3*, 28.
(26) Brown, D. W.; Lowry, R. E.; Smith, L. E. *Macromolecules* **1980**, *13*, 248.
(27) Zimmerman, H.; Kim, N. T. *Polym. Eng. Sci.* **1980**, *20*, 680.
(28) Schmitt, E. A.; Flanagan, D. R.; Linhardt, R. J. *J. Pharm. Sci.* **1993**, *82*, 326.
(29) Lofgren, A.; Albertsson, A. C. *J. Appl. Polym. Sci.* **1994**, *52*, 1327.
(30) Bellenger, V.; Ganem, M.; Mortaigne, B.; Verdu, J. *Polym. Degrad. Stab.* **1995**, *49*, 91.
(31) Farrow, N. A.; Muhandiram, R.; Singer, A. U.; Pascal, S. M.; Kay, C. M.; Gish, G.; Shoelson, S. E.; Pawson, T.; Forman-Kay, J. D.; Kay, L. E. *Biochemistry* **1994**, *33*, 5984.
(32) Fagerness, P. E.; Grant, D. M.; Kuhlmann, K. F.; Mayne, C. L.; Parry, R. B. *J. Chem. Phys.* **1975**, *63*, 2524.
(33) Vold, R. R.; Vold, R. L. *J. Chem. Phys.* **1976**, *64*, 320.
(34) Cavanagh, J.; Rance, M. *J. Magn. Reson.* **1992**, *96*, 670.
(35) Bax, A.; Ikura, M.; Kay, L. E.; Torchia, D. A.; Tschudin, R. *J. Magn. Reson.* **1990**, *86*, 304.
(36) Zhang, O. W.; Kay, L. E.; Olivier, J. P.; Forman-Kay, J. D. *J. Biomol. NMR* **1994**, *4*, 845.
(37) Braunschweiler, L.; Ernst, R. R. *J. Magn. Reson.* **1983**, *53*, 521.
(38) Kogler, H.; Sorensen, O. W.; Bodenhausen, G.; Ernst, R. R. *J. Magn. Reson.* **1983**, *55*, 157.
(39) Ikura, M.; Bax, A. *J. Am. Chem. Soc.* **1992**, *114*, 2433.
(40) Dayie, K. T.; Wagner, G. *J. Magn. Reson. A* **1994**, *111*, 121.
(41) Meersmann, T.; Bodenhausen, G. *J. Magn. Reson. A* **1995**, *115*, 277.
(42) Mabey, W.; Mill, T. *J. Phys. Chem. Ref. Data* **1978**, *7*, 383.
(43) VanVranken, D. L.; Panomitros, D.; Schultz, P. G. *Tetrahedron Lett.* **1994**, *35*, 3873.
(44) Chapman, T. M. *J. Polym. Sci., Part A* **1989**, *27*, 1993.
(45) Vontor, T.; Vecera, M. *Collect. Czech. Chem. Commun.* **1973**, *38*, 516.
(46) Drossman, H.; Johnson, H.; Mill, T. *Chemosphere* **1988**, *17*, 1509.
(47) Pegoretti, A.; Kolarik, J.; Penati, A. *Angew. Makromol. Chem.* **1994**, *220*, 49.
(48) Marion, D.; Ikura, M.; Tschudin, R.; Bax, A. *J. Magn. Reson.* **1989**, *85*, 393.
(49) Cavanagh, J.; Palmer, A. G.; Wright, P. E.; Rance, M. *J. Magn. Reson.* **1991**, *91*, 429.
(50) Kay, L. E.; Keifer, P.; Saarinen, T. *J. Am. Chem. Soc.* **1992**, *114*, 10663.

MA992030W